J. Fluid Mech. (2000), *vol.* 419, *pp.* 239–262. Printed in the United Kingdom

Linear stability analysis of channel inception: downstream-driven theory

By NORIHIRO IZUMI[1]† AND GARY PARKER[2]

[1]Department of Civil Engineering, Tohoku University, Sendai, 980–8579, Japan
[2]St. Anthony Falls Laboratory, University of Minnesota, Minneapolis, MN 55414, USA

(Received 8 December 1998 and in revised form 16 May 2000)

A linear stability analysis of incipient channellization on hillslopes is performed using the shallow-water equations and a description of the erosion of a cohesive bed. The base state consists of a laterally uniform Froude-subcritical sheet flow down a smooth, downward-concave hillslope profile. The downstream boundary condition consists of the imposition of a Froude number of unity. The process of channellization is thus driven from the downstream end. The flow and bed profiles describe a base state that migrates at constant, slow speed in the upstream direction due to bed erosion. Transverse perturbations corresponding to a succession of parallel incipient channels are introduced. It is found that these perturbations grow in time, so describing incipient channellization, only when the characteristic spacing between incipient channels is on the order of 6–100 times the Froude-critical depth divided by the resistance coefficient. The characteristic wavelength associated with maximum perturbation growth rate is found to scale as 10 times the Froude-critical depth divided by the resistance coefficient. Evaluating the friction coefficient as on the order of 0.01, an estimate of incipient channel spacing on the order of 1000 times the Froude-critical depth is obtained. The analysis reveals that downstream-driven channellization becomes more difficult as (*a*) the critical shear stress required to erode the bed becomes so large that it approaches the Froude-critical shear stress reached at the downstream boundary and (*b*) the Froude number of the subcritical equilibrium flow attained far upstream approaches unity. Alternative mechanisms must be invoked to explain channellization on slopes high enough to maintain Froude-supercritical sheet flow.

1. Introduction

An erodible slope subjected to rainfall tends to become dissected by channels which in the initial stages of development are often roughly parallel and uniformly spaced in the transverse direction. This process of incipient channellization can be commonly observed in nature at a variety of scales, from the small rills that form on freshly formed slopes adjacent to roads (e.g. Sawai 1977) to larger natural channels that form on hillslopes (e.g. Montgomery & Dietrich 1989; Reid 1989). An illustration of naturally evolved channel spacing is given in figure 1.

Significant progress on the evolution of channelized drainage basins has been made since the early research due to Smith & Bretherton (1972) and Luke (1974). In particular, Willgoose, Bras & Rodriguez-Iturbe (1991*a*, *b*) offered the first numerical model capable of reproducing the evolution of complete channelized drainage basins

† Present address: School of Civil Engineering, Asian Institute of Technology, Pathumthani 12120, Thailand.

FIGURE 1. Illustration of channellization with a characteristic transverse spacing between channels. The lake is Mangoku Lagoon near Sendai, Japan.

from slopes that are initially flat except for randomized perturbations. Significant further progress has been made by Howard (1994) and Tucker & Slingerland (1997). A summary of developments in the modelling of channellization and drainage basin formation can be found in Rodriguez-Iturbe & Rinaldo (1997).

A characteristic feature of the above models is that they rely on a cellular discretization of the problem. Within this discretization the equations of flow momentum balance are approximated simply by the formulation for steady, uniform flow, i.e. normal flow, applied down the steepest path of descent. These cellular models are of considerable value because (*a*) they evolve complex topography from a relatively small number of physically based rules and (*b*) they allow studies of varied hydrologic regime, tectonic environment etc. They are not, however, capable of answering all questions that might be asked about channellization.

In particular, cellular models rely on the addition of random perturbations to an initially flat, tilted surface in order to start the process of channellization. The pattern of initial channellization is a function of the randomization. That is, the models do not appear to encompass an inherent instability that causes flat, tilted surfaces subject to sheet flow to begin channellization in a characteristic way. The goal of the present paper is a rigorous description of such an instability.

Two basic scenarios have been considered for the process of incipient channellization. The first of these is an 'upstream-driven' scenario which relies on direct erosion of the hillslope itself. Sheet flow on a slope cannot be expected to be perfectly uniform. Instead, interaction between the tendency for the flow to concentrate and the tendency for the bed to erode in such zones of concentration might be expected to give rise to a characteristic spacing between incipient channels. The first attempt at a linear stability analysis of channellization, that due to Smith & Bretherton (1972), was of this type. Their groundbreaking work has served to motivate much of the more recent research on drainage basin evolution. Their formulation of the flow, however, consisted simply of the assumption of steady, uniform (i.e. normal) open channel flow. This proved too simple to characterize the problem, and as a result the predicted characteristic spacing between channels proved to be infinitely small. Loewenherz (1991) was evidently aware of this shortcoming of the model of Smith & Bretherton. Her model, however, relied on the introduction of artificial terms into the equations of motion in order to obtain a finite characteristic spacing.

Izumi & Parker (1995*a*) approached this scenario using the full shallow-water equations of open channel flow. In their linear analysis the flow is allowed to gather in parallel downslope-directed infinitesimal troughs of arbitrary transverse spacing. Overall flow increases in the downstream direction due to rainfall. Near the top of the ridge, the flow is assumed to be too weak to erode the bed, but as discharge increases downslope a point is reached after which erosion can occur. The model predicts the transverse spacing between channels as being the one which causes erosion at the farthest upstream point in the troughs. This spacing scales with the depth of the sheet flow divided by the slope of the surface. The analysis successfully overcomes the limitations of steady, uniform flow in predicting incipient channel spacing. Because it quantifies the process in terms of the inception rather than the rate of erosion, however, the analysis cannot be classified as a formal stability analysis.

The second scenario for the process of incipient channellization is 'downstream-driven', according to which the process is partly controlled at a point at the downstream end of the hillslope. For example, in the case for which the hillslope terminates in a free overfall, the sheet flow must form a backwater curve as it accelerates toward the precipice. As a result intense erosion might be expected just upstream of the precipice. Again, it can be expected that this erosion would not be completely uniform in the transverse direction; instead, interaction between flow concentration and bed erosion should give rise to a characteristic spacing between incipient channels. The authors are aware of only one paper treating this scenario, that of Izumi & Parker (1995*b*). The analysis, which employs same type of perturbation as that of Izumi & Parker (1995*a*), again relies upon considerations of incipient erosion, and does not describe erosion itself. Although it yields an incipient spacing between channels that scales with sheet flow depth divided by slope, it is not a formal stability analysis. In addition, it must rely on a description of incipient erosion upstream of the precipice, where the analysis becomes singular.

In the present paper these shortcomings of the downstream-driven scenario are overcome through the use of a formal linear stability analysis of an erodible bed. In this way the model not only encompasses the tendency of the flow to gather in low areas, but also describes the time process of channel erosion as it interacts with the flow. It provides a rigorous and physically sound basis for determining the transverse spacing between channels. It should be noted, however, that a linear stability analysis can predict channel spacing only at the inception of channellization. Nonlinear effects can be expected to change the spacing, most likely in the direction of

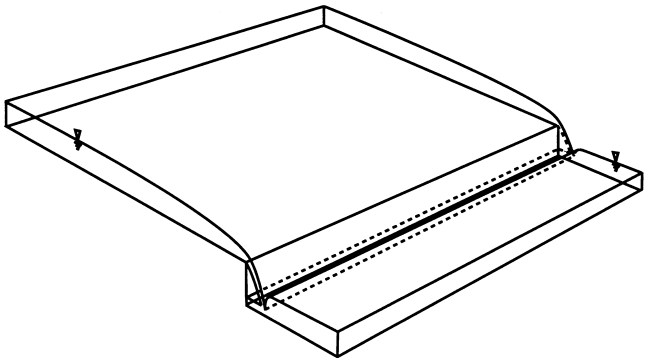

FIGURE 2. Definition diagram for flow over a vertical precipice.

longer wavelength as the upstream flow to weaker channels is arrogated by stronger channels.

2. The conceptual model

The conceptual model of Izumi & Parker (1995*b*) is reviewed first. Consider an erodible surface with a constant slope S in the $\tilde{x}$ (downslope) direction and vanishing slope in the $\tilde{y}$ (transverse) direction, as described in figure 2. In this paper the tildes denote terms with dimensions. The surface is subjected to a rainfall, which induces a sheet flow the intensity of which increases in the downslope direction. The downslope increase in flow intensity must be specifically included in any upstream-driven model of channellization, e.g. Izumi & Parker (1995*a*). In the case of the present downstream-driven model, however, the length of influence of the precipice on the flow extends upstream a distance that scales with flow depth divided by slope. As shown in Izumi & Parker (1995*b*), as long as this distance is short compared to the length of the slope from precipice to ridge crest the effect of rainfall can be ignored in the vicinity of the precipice. With this in mind, it is assumed that before the development of channellization the water discharge per unit width q is constant in both the streamwise and transverse directions.

The slope S is taken to be sufficiently low to ensure that the flow upstream of the precipice is always in the subcritical Froude regime. (The upstream-driven analysis of Izumi & Parker 1995*a* is appropriate for supercritical overland flow.) Such a flow must accelerate toward a Froude number of unity at the precipice of the overfall. If in the process of doing so the boundary shear stress somewhere exceeds the threshold value for erosion, the region from the precipice upstream to the beginning of erosion must begin to deform. This deformation can be expected to gradually propagate upslope. In the absence of any lateral perturbations this upslope translation should be uniform in the transverse direction. Local low zones along the precipice can, however, be expected to gather more flow, resulting in higher erosion rates and the inception of channellization.

The conceptual basis for the present downstream-driven model is similar to that of Izumi & Parker (1995*b*), but different in an important way. As can be seen in figure 1, it is common to find that the ridges between channels form a downward-concave profile, such that slope increases in the downslope direction. As erosion is likely to be least on the ridges, they provide an idea as to what the slope might be like in the absence of channellization. The base state before the introduction of perturbations in

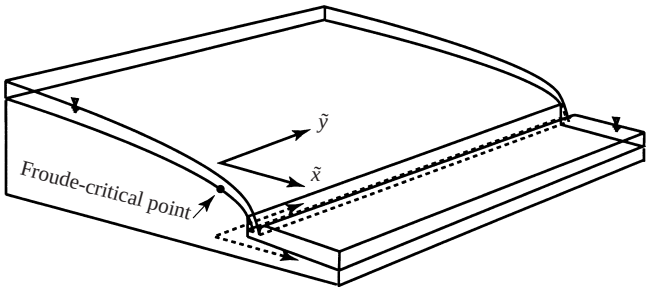

FIGURE 3. Definition diagram for flow over a downward-concave slope, with subcritical flow for $\tilde{x} < 0$ (the domain of interest in the present analysis).

the transverse direction is here taken to be a downward concave profile of the type of figure 3.

Herein this downward-concave base profile is not chosen arbitrarily. Instead, it is taken to be a self-preserving form that propagates in the upslope direction at constant speed in response to erosion. It establishes the starting point for a true stability analysis of incipient downstream-driven channellization.

This base state is introduced in Parker & Izumi (2000), where it is termed a solitary step. Here the analysis is extended considerably. While a rigorous analysis follows below, it is useful to describe in advance several characteristics of the profile. The profile links the flow pattern with the profile of bed elevation. Far upstream the profile attains a constant bed slope S_n associated with normal Froude-subcritical flow at constant velocity. The analysis also applies to the limiting case of vanishing S_n, in which case the streamwise velocity profile converges to the spatially varying form over a horizontal bed far upstream. Both bed slope and streamwise flow velocity increase monotonically downstream to a point where the Froude number attains unity, as shown in figure 3. This point of Froude-critical flow defines the downstream boundary condition for the present downstream-driven theory.

The analysis of the base state presented here represents a considerable generalization over that presented in Parker & Izumi (2000). Three limiting cases are possible far upstream: one for which the bed is eroding, one for which the bed is at the threshold conditions for erosion and one for which the bed is not eroding. In the last of these three, the zone of eroding bed extends only a finite distance upstream of the Froude-critical point. The stability analysis for incipient channellization presented here applies to all three cases.

In order to perform a linear stability analysis transverse perturbations are introduced into the base state. A sinusoidal perturbation with wavenumber $\tilde{k}$ is given at the precipice of the downstream end of the slope, as shown in figure 4. In the case of subcritical overland flow, the local troughs should attract the flow, causing a gathering of streamlines. The protuberances should exert a comensurate repulsion of the flow. This causes amplification of the boundary shear stress in the troughs, which in turn amplifies the rate of bed erosion in them. The resulting incision characterizes the mode of channellization envisioned here. The incipient channels grow through the self-reinforcing interaction of the focusing of flow down troughs and incision. The characteristic wavelength $\tilde{\lambda}_m (= 2\pi/\tilde{k}_m)$ at which the growth rate is maximized is expected to be the dominant spacing of the incipient channels. In the case where the bed of the base state is eroding only a finite distance upstream of the Froude-critical point, the bed perturbations extend only the same finite distance upstream. This

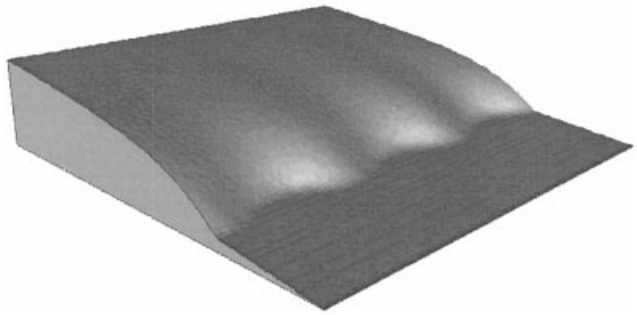

FIGURE 4. Conceptual diagram showing the introduction of transverse perturbations representing incipient channellization into the slope profile of figure 3.

does not mean that channellization cannot propagate farther up the slope, but rather relegates the study of this phenomenon to a fully nonlinear finite-amplitude analysis.

3. Analytical formulation

3.1. *Governing equations*

The present analysis is devoted to a description of the non-steady process by which an erosional surface evolves in response to sheet flow. A changing surface implies a changing flow. This notwithstanding, if the time scale associated with surface evolution in response to erosion is long compared to that associated with the response of the flow to the changing surface, the classical quasi-steady approximation can be invoked. This approximation, according to which the unsteady terms in the equations of motion of the flow can be neglected, is adopted here. The shallow-water equations associated with two-dimensional sheet flow thus take the following form:

$$\tilde{u}\frac{\partial \tilde{u}}{\partial \tilde{x}} + \tilde{v}\frac{\partial \tilde{u}}{\partial \tilde{y}} = -g\frac{\partial \tilde{h}}{\partial \tilde{x}} - g\frac{\partial \tilde{\eta}}{\partial \tilde{x}} - \frac{\tilde{\tau}_x}{\rho \tilde{h}}, \tag{3.1}$$

$$\tilde{u}\frac{\partial \tilde{v}}{\partial \tilde{x}} + \tilde{v}\frac{\partial \tilde{v}}{\partial \tilde{y}} = -g\frac{\partial \tilde{h}}{\partial \tilde{y}} - g\frac{\partial \tilde{\eta}}{\partial \tilde{y}} - \frac{\tilde{\tau}_y}{\rho \tilde{h}}, \tag{3.2}$$

$$\frac{\partial \tilde{u}\tilde{h}}{\partial \tilde{x}} + \frac{\partial \tilde{v}\tilde{h}}{\partial \tilde{y}} = 0. \tag{3.3}$$

In the above relations $(\tilde{x}, \tilde{y})$ are the streamwise and lateral coordinates in the horizontal plane shown in figure 3; $(\tilde{u}, \tilde{v})$ and $(\tilde{\tau}_x, \tilde{\tau}_y)$ denote the depth-averaged flow velocity and boundary shear stress in the $(\tilde{x}, \tilde{y})$ direction, $\tilde{h}$ denotes flow depth, $\tilde{\eta}$ denotes bed elevation, ρ denotes the density of water and g denotes gravitational acceleration. The above form of the equations of motion is valid as long as the bed slope is not too steep and the flow is not changing too rapidly in the streamwise direction.

The description of sediment continuity appropriate for the analysis of channel processes can be broadly divided into two classes, i.e. transportational and erosional formulations (Izumi & Parker 1995*b*). In the former description the erodible bed surface is taken to be non-cohesive and erosion and deposition of sediment are assumed to occur simultaneously, giving rise to a vector of volume bedload transport per unit width $\boldsymbol{q}_B$ which is always directed tangential to the surface. The associated

Exner equation of sediment continuity is

$$\frac{\partial \tilde{\eta}}{\partial \tilde{t}} = -\frac{1}{1-\lambda_p}\tilde{\nabla}\cdot \boldsymbol{q}_B, \tag{3.4a}$$

where $\tilde{t}$ denotes time, λ_p denotes the porosity of the sediment composing the bed surface and $\tilde{\nabla}$ denotes the dimensioned form of the standard nabla operator. This formulation, which is the basis for the analysis of e.g. Smith & Bretherton (1972), Luke (1974) and Willgoose *et al.* (1989), is appropriate for the case when the channels have evolved to the point that their beds are covered by a layer of non-cohesive sediment. This 'transportational' formulation, however, results in a description of flow over an erodible bed that has a strongly diffusional component. For this reason it cannot describe the downward-concave base profile observed in the field (the ridges of figure 1) and schematized in figure 2.

An alternative formulation would appear to be more appropriate for a study of channel inception. As is demonstrated in the next section, a purely erosional formulation can be used to describe a downward concave profile that can in turn be used as the base state for a stability analysis of incipient channellization. In this formulation, the regolith that composes the erodible sediment layer below the surface is assumed to be cohesive. Once detached, however, the sediment is assumed to be carried far downstream by the flow (and in particular well downstream of the Froude-critical point of figure 3) before depositing, resulting in long reaches which are purely erosional. These conditions should hold when the erosion rate is sufficiently small, and when storm-driven flows have a capacity to transport sediment on hillslopes that far exceeds the delivery through erosion. In the present treatment this purely erosional formulation is considered. The Exner equation of conservation of bed sediment takes the form

$$\frac{\partial \tilde{\eta}}{\partial \tilde{t}} = -\tilde{E}(\tilde{\tau}), \tag{3.4b}$$

where $\tilde{E}$ denotes the velocity of erosion of the bed due to the flow of water. In most formulations to date this parameter is taken to be a power function of the magnitude $\tilde{\tau}$ of the boundary shear stress vector, such that

$$\tilde{E}(\tilde{\tau}) = \begin{cases} \alpha((\tilde{\tau}/\tilde{\tau}_{th}) - 1)^{\gamma} & \text{if} \quad \tilde{\tau} \geqslant \tilde{\tau}_{th} \\ 0 & \text{if} \quad \tilde{\tau} < \tilde{\tau}_{th}, \end{cases} \tag{3.5a}$$

$$\tilde{\tau} = (\tilde{\tau}_x^2 + \tilde{\tau}_y^2)^{1/2}, \tag{3.5b}$$

where $\tilde{\tau}_{th}$ denotes the critical or threshold value of $\tilde{\tau}$ for the onset of bed erosion (not to be confused with the Froude-critical condition), γ denotes a dimensionless exponent and α is a parameter with the dimensions of velocity (Ariathurai & Arulanandan 1978; Sheng & Lick 1978; Parker & Izumi 2000). Both these parameters are functions of soil type and conditions. Empirical determinations of γ generally place it in the range 0.5–4. It will be shown in the present analysis that physically realistic solutions cannot be realized for $\gamma < 1$, implying that channellization cannot occur by the present mechanism if the erosion rate depends too weakly on the magnitude of the boundary shear stress vector.

Here the boundary shear stress is related to flow velocity by means of a friction coefficient C_f:

$$(\tilde{\tau}_x, \tilde{\tau}_y) = \tilde{\tau}\frac{(\tilde{u}, \tilde{v})}{(\tilde{u}^2 + \tilde{v}^2)^{1/2}}, \qquad \tilde{\tau} = \rho C_f(\tilde{u}^2 + \tilde{v}^2). \tag{3.6a, b}$$

In general C_f is a weak function of flow depth and roughness height, but in the present theory it is taken to be a given constant for simplicity.

The domain of solution is $(-\infty, \tilde{x}_c)$ where $\tilde{x}_c$ denotes the point at which Froude-critical conditions are reached. Appropriate upstream and downstream conditions can be set as follows. Far upstream the flow should attain steady, uniform normal conditions, and the bed slope should approach a constant slope S_n. The downstream-driven channellization described herein will be shown to decay to zero far upstream, so that the following conditions are satisfied:

$$(\tilde{u}, \tilde{v}) \to (\tilde{u}_n, 0), \qquad -\frac{\partial \tilde{\eta}}{\partial \tilde{x}} \to S_n \quad \text{as} \quad \tilde{x} \to -\infty, \tag{3.7a, b}$$

where $\tilde{u}_n$ is obtained from the steady, uniform approximation obtained from (3.1) and (3.3) with the aid of (3.6):

$$C_f \tilde{u}_n^2 = g\tilde{h}_n S_n, \quad \tilde{u}_n \tilde{h}_n = q. \tag{3.7c, d}$$

As will be seen from the solution for the base flow, (3.7a, b) are not formally boundary conditions; if the problem is set up correctly they will be found to be automatically satisfied.

The profiles of figures 3 and 4 will be shown to become monotonically steeper in the downslope ($\tilde{x}$) direction, ensuring that Froude-critical conditions are reached at some point $\tilde{x}_c$, where the bed elevation $\tilde{\eta}$ is taken to vanish for simplicity. Thus where the Froude number Fr is denoted as

$$Fr = \left(\frac{\tilde{u}^2 + \tilde{v}^2}{g\tilde{h}} \right)^{1/2}, \tag{3.8a}$$

it follows that

$$Fr = 1, \quad \tilde{\eta} = 0 \quad \text{at} \quad \tilde{x} = \tilde{x}_c. \tag{3.8b, c}$$

In the solution for the base state it will be found that the point $\tilde{x}_c$ migrates upstream at constant speed. The above equations constitute formal boundary conditions for the problem.

It is useful to introduce three dimensionless parameters at this point. Equation (3.7c) can be expressed in the form

$$Fr_n^2 = \sigma, \tag{3.9a}$$

where Fr_n denotes the Froude number associated with normal flow far upstream and σ denotes a normalized slope far upstream, such that

$$Fr_n = \frac{\tilde{u}_n}{(g\tilde{h}_n)^{1/2}}, \quad \sigma = \frac{S_n}{C_f}. \tag{3.9b, c}$$

The shear stress $\tilde{\tau}_n$ realized at the normal flow far upstream is given by

$$\tilde{\tau}_n = \rho C_f \tilde{u}_n^2. \tag{3.10a}$$

The ratio of the critical shear stress for bed erosion to the normal bed shear stress is here defined to be ψ_n, where

$$\psi_n = \frac{\tilde{\tau}_{th}}{\tilde{\tau}_n}. \tag{3.10b}$$

The range of validity of the present analysis is thus

$$0 < Fr_n < 1. \tag{3.11}$$

The case $\psi_n < 1$ corresponds to one for which erosion extends infinitely far upstream in the base state; when $\psi_n > 1$ erosion extends only a finite distance upstream.

3.2. *Non-dimensionalization*

The governing equations are rendered dimensionless using scales associated with the one-dimensional (laterally uniform) base flow over the configuration of figure 3. This base flow is characterized by a constant water discharge per unit width q. The following transformations are introduced in order to remove dimensions from the problem; the parameters without tildes are the dimensionless versions of the corresponding parameters with tildes:

$$(\tilde{u}, \tilde{v}) = U_c(u, v), \quad (\tilde{x}, \tilde{y}) = \frac{D_c}{C_f}(x, y), \quad (\tilde{h}, \tilde{\eta}) = D_c(h, \eta), \tag{3.12a–c}$$

$$\tilde{k} = \left(\frac{D_c}{C_f}\right)^{-1} k, \quad \tilde{t} = D_c \left[\alpha \left(\frac{\tilde{\tau}_c}{\tilde{\tau}_{th}}\right)^{\gamma}\right]^{-1} t, \quad \tilde{\tau}_c = \rho C_f U_c^2. \tag{3.12d–f}$$

In the above relations U_c and D_c denote the flow velocity and depth of the base flow corresponding to Froude-critical flow conditions, i.e. for which

$$Fr = \frac{\tilde{u}}{(g\tilde{h})^{1/2}} = 1. \tag{3.13a}$$

It is easily shown from the above relation and the condition of flow continuity that U_c and D_c must take the forms

$$U_c = (qg)^{1/3}, \quad D_c = \left(\frac{q^2}{g}\right)^{1/3}. \tag{3.13b, c}$$

Introducing (3.12*a–f*) into (3.1)–(3.3) and (3.4*b*) and reducing, the following dimensionless relations are obtained:

$$u\frac{\partial u}{\partial x} + v\frac{\partial u}{\partial y} = -\frac{\partial h}{\partial x} - \frac{\partial \eta}{\partial x} - \frac{\left(u^2 + v^2\right)^{1/2} u}{h}, \tag{3.14}$$

$$u\frac{\partial v}{\partial x} + v\frac{\partial v}{\partial y} = -\frac{\partial h}{\partial y} - \frac{\partial \eta}{\partial y} - \frac{\left(u^2 + v^2\right)^{1/2} v}{h}, \tag{3.15}$$

$$\frac{\partial uh}{\partial x} + \frac{\partial vh}{\partial y} = 0, \tag{3.16}$$

$$\frac{\partial \eta}{\partial t} = -E(u^2 + v^2). \tag{3.17}$$

In (3.17) E denotes the dimensionless rate of bed erosion, given by

$$E(u^2 + v^2) = \begin{cases} (u^2 + v^2 - \psi)^{\gamma} & \text{if} \quad u^2 + v^2 \geqslant \psi \\ 0 & \text{if} \quad u^2 + v^2 < \psi, \end{cases} \tag{3.18}$$

where ψ denotes the ratio of the critical shear stress for bed erosion to the shear stress realized at Froude-critical conditions:

$$\psi = \frac{\tilde{\tau}_{th}}{\tilde{\tau}_c}. \tag{3.19a}$$

This parameter, which must always be less than unity, is related to ψ_n as follows:

$$\psi = u_n^2 \psi_n, \tag{3.19b}$$

where u_n denotes the dimensionless normal flow velocity far upstream, which from (3.7c, d) and (3.9) is found to satisfy the relations

$$u_n = \sigma^{1/3} = Fr_n^{2/3}. \tag{3.19c}$$

A corresponding non-dimensionalization of (3.7a, b) and (3.8b, c) yields the upstream and boundary conditions

$$(u, v) \to (u_n, 0), \quad -\frac{\partial \eta}{\partial x} \to \sigma \quad \text{as} \quad x \to -\infty, \tag{3.20a, b}$$

$$u^2 + v^2 = h, \quad \eta = 0 \quad \text{at} \quad x = x_c. \tag{3.21a, b}$$

4. The one-dimensional base state

4.1. *Formulation and coordinate transformation*

The dimensionless equations of the base state are obtained from (3.14)–(3.17) by assuming the flow to be solely in the $\tilde{x}$-direction and assuming $\tilde{v}$ to vanish:

$$u\frac{\partial u}{\partial x} = -\frac{\partial h}{\partial x} - \frac{\partial \eta}{\partial x} - \frac{u^2}{h}, \tag{4.1}$$

$$uh = 1, \tag{4.2}$$

$$\frac{\partial \eta}{\partial t} = -E(u^2). \tag{4.3}$$

As noted earlier, a solution is sought which describes a profile that retreats at a constant speed in the x-direction while maintaining an invariant profile. This solution offers two advantages. First, it describes the downward-concave profile of figure 3, which is in general agreement with the observation that the ridges between channels, which can be taken to be relicts of a previous unchannelized state, are typically observed to be downward concave. Secondly, the solution of permanent form resulting from the assumption of a constant upstream migration rate describes an equilibrium that provides a convenient base state for a formal stability analysis. It is not meant to imply here that channellization always begins from this particular base state. Rather, it is argued that this base state is a realistic one from which a rigorous stability analysis can be conducted. The following coordinate transformations are introduced to this end:

$$\eta^* = \eta - bt, \quad x^* = x + ct, \quad t^* = t. \tag{4.4a–c}$$

In (4.4b) c denotes the constant velocity of migration of the profile in the upstream direction and b is a constant necessitated by the fact that the bed is eroding everywhere when $\psi_n < 1$. Introducing (4.4a–c) into (4.1)–(4.3), dropping the dependence on time t^* and dropping the stars for simplicity, it is found that (4.1) and (4.2) remain unchanged, whereas (4.3) reduces to

$$c\frac{\mathrm{d}\eta}{\mathrm{d}x} + b = -E(u^2), \quad E(u^2) = \begin{cases} (u^2 - \psi)^\gamma & \text{for } u^2 > \psi \\ 0 & \text{for } u^2 \leqslant \psi. \end{cases} \tag{4.5a, b}$$

The following three cases can be distinguished with the aid of (3.19b), (3.19c) and

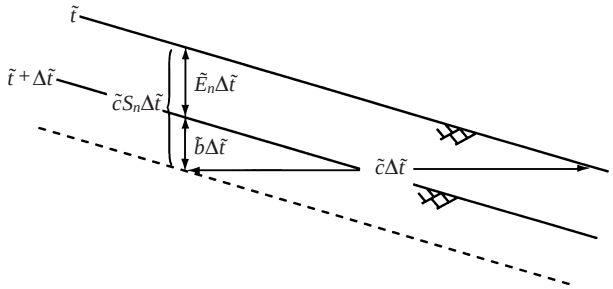

FIGURE 5. Diagram showing the physical interpretation of $\tilde{b}$.

(4.5*b*). In the case $u_n^2 > \psi$, i.e. $\psi_n < 1$, erosion extends infinitely far upstream. In the case $u_n^2 = \psi$, i.e. $\psi_n = 1$, the threshold condition for erosion is reached infinitely far upstream. In the case $u_n^2 < \psi$, i.e. $\psi_n > 1$, erosion extends only a finite distance upstream. In this last case it will be found that η converges to a profile with a constant slope at a finite distance upstream of the Froude-critical point, whereas u converges to u_n only at $x = -\infty$. The present analysis encompasses all three cases.

The constant b can be obtained by considering flow far upstream where normal conditions are maintained, for which case $\mathrm{d}\eta/\mathrm{d}x \to -\sigma$ and $E \to E_n$, where σ denotes the normalized upstream slope and E_n denotes the dimensionless erosion rate under normal conditions far upstream. With the use of (3.19*b*) and (3.19*c*) it is found that

$$E_n = \begin{cases} (u_n^2 - \psi)^\gamma & \text{for } u_n^2 > \psi \\ 0 & \text{for } u_n^2 \leqslant \psi \end{cases} = \begin{cases} [Fr_n^{4/3}(1-\psi_n)]^\gamma & \text{for } \psi_n < 1 \\ 0 & \text{for } \psi_n \geqslant 1. \end{cases} \tag{4.6}$$

Thus far upstream (4.5*a*) reduces to

$$b = c\sigma - E_n. \tag{4.7}$$

Substitution of (4.7) into (4.5*a*) yields

$$\frac{\mathrm{d}\eta}{\mathrm{d}x} = -\sigma - c^{-1}[E(u^2) - E_n]. \tag{4.8}$$

While the parameter b is easily obtained through the above formal manipulation of the equations, its physical meaning is best expressed by briefly returning to dimensioned parameters and considering the normal flow conditions assumed to be realized far upstream. Let $\tilde{c}$ denote the dimensional version of dimensionless wave speed c. In time $\Delta\tilde{t}$ a Lagrangian point in the bed elevation profile is moved upstream a distance $\tilde{c}\Delta\tilde{t}$, where it is now a distance $\tilde{c}S_n\Delta\tilde{t}$ below the original bed profile at time $\tilde{t}$. During this time the bed will have eroded down a distance $\tilde{E}_n\Delta\tilde{t}$. In general, however the distance $\tilde{E}_n\Delta\tilde{t}$ will not be equal to $\tilde{c}\Delta\tilde{t}$. In order for the Lagrangian point to be at the correct elevation, the parameter $\tilde{b}$ must be introduced so that the following condition holds:

$$\tilde{E}_n\Delta\tilde{t} + \tilde{b}\Delta\tilde{t} = \tilde{c}S_n\Delta\tilde{t}, \tag{4.9}$$

or the dimensionless form (4.7). The relation between the various parameters in (4.9) is illustrated in figure 5.

Reduction of (4.1) and (4.2) with (4.4) yields the relation

$$\frac{\mathrm{d}u}{\mathrm{d}x} = \frac{u^5 + u^2\mathrm{d}\eta/\mathrm{d}x}{1-u^3}. \tag{4.10}$$

The upstream and boundary conditions on (4.8) and (4.10) are expressed as follows.

The downstream boundary $\tilde{x}_c$ at which Froude-critical flow is realized is assumed to migrate upstream at the same speed c as the rest of the profile, so that it can be specified as the point $x = 0$ in the moving coordinate system without loss of generality. Thus (3.8b, c) reduce to the respective boundary conditions

$$u|_{x=0} = 1, \quad \eta|_{x=0} = 0, \tag{4.11a, b}$$

and (3.7a) reduces to the upstream condition

$$u|_{x=-\infty} = u_n. \tag{4.12}$$

4.2. *Solution for the base state*

Substituting (4.8) into (4.10) and reducing, it is found that

$$\frac{\mathrm{d}u}{\mathrm{d}x} = \frac{u^5 - u^2\{\sigma + c^{-1}[E(u^2) - E_n]\}}{1 - u^3}. \tag{4.13}$$

Note that the denominator on the right-hand side of the equation vanishes at the origin $x = 0$, where Froude-critical conditions are realized. The smooth profile of figure 3 indicates, however, that there should be no singularity in $\mathrm{d}u/\mathrm{d}x$ at the point at which Froude-critical flow is realized (e.g. Escoffier 1958; Chow 1959). With this in mind, the numerator must vanish as well at the origin, thus specifying the migration speed c:

$$c = \frac{E_o - E_n}{1 - \sigma}, \tag{4.14a}$$

where

$$E_o = E|_{x=0} = (1 - \psi)^{\gamma}. \tag{4.14b}$$

Expressing c purely in terms of the parameters Fr_n and ψ, it is found from (3.19c), (4.6) and (4.14) that

$$c = \begin{cases} \dfrac{(1-\psi)^{\gamma} - (Fr_n^{4/3} - \psi)^{\gamma}}{1 - Fr_n^2} & \text{for } Fr_n^{4/3} - \psi > 0 \\ \dfrac{(1-\psi)^{\gamma}}{1 - Fr_n^2} & \text{for } Fr_n^{4/3} - \psi \leqslant 0. \end{cases} \tag{4.15}$$

Starting from (4.7), a similar reduction for b yields the form

$$b = \begin{cases} Fr_n^2 \dfrac{(1-\psi)^{\gamma} - (Fr_n^{4/3} - \psi)^{\gamma}}{1 - Fr_n^2} - (Fr_n^{4/3} - \psi)^{\gamma} & \text{for } Fr_n^{4/3} - \psi > 0 \\ Fr_n^2 \dfrac{(1-\psi)^{\gamma}}{1 - Fr_n^2} & \text{for } Fr_n^{4/3} - \psi \leqslant 0. \end{cases} \tag{4.16}$$

Substituting (4.14a) into (4.13) and reducing, it is found that

$$\frac{\mathrm{d}u}{\mathrm{d}x} = \frac{u^5 - u^2\left\{\sigma + (1-\sigma)[E(u^2) - E_n]/[E_o - E_n]\right\}}{1 - u^3}. \tag{4.17}$$

It is readily seen from (3.19c) and (4.17) that $\mathrm{d}u/\mathrm{d}x \to 0$ as $u \to u_n$, indicating that the upstream condition (4.12) is satisfied perforce. The form of $\mathrm{d}u/\mathrm{d}x$ remains, however, indeterminate at $x = 0$. An application of L'Hopital's rule yields the result

$$u_{x0} \equiv \left.\frac{\mathrm{d}u}{\mathrm{d}x}\right|_{x=0} = 1 - \tfrac{1}{3}(1-\sigma)\frac{2\gamma(1-\psi)^{\gamma-1}}{(1-\psi)^{\gamma} - E_n}. \tag{4.18}$$

The parameter u_{x0} must be positive in order to yield the physically realistic condition

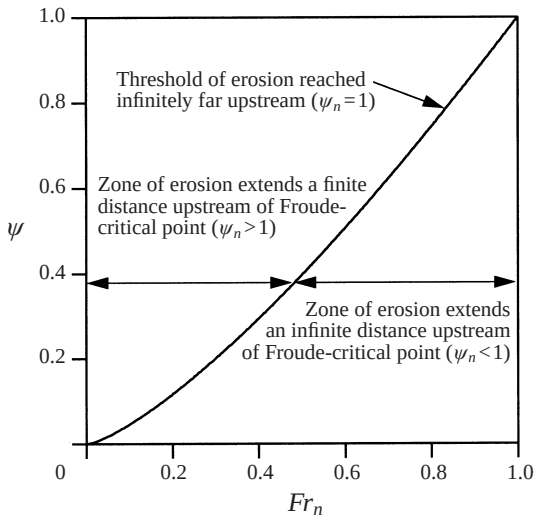

FIGURE 6. Regime diagram showing the range of values of Fr_n and ψ for which erosion extends infinitely far upstream, and the range for which it does not.

of flow that is accelerating in the downstream direction at the Froude-critical point. In the case for which $E_n > 0$, corresponding to erosion extending infinitely far upstream, the exponent γ must generally be in excess of a value between 1 and 1.5 in order for this condition to hold. When $E_n = 0$, corresponding to erosion extending a finite distance upstream, u_{x0} is generally positive even for values of γ below unity.

Equation (4.17) can now be solved with the aid of (4.11*a*) and (4.18) upon specification of three parameters: the exponent γ in the erosion relation, the normal Froude number Fr_n attained far upstream (or alternatively the normalized upstream slope σ) and the ratio ψ of critical shear stress for bed erosion to the shear stress at Froude-critical conditions. The integration proceeds upstream from $x = 0$. Once the solution for u is known, the elevation profile $\eta(x)$ can be obtained by integrating (4.8) subject to (4.11*b*).

4.3. *Evaluation of the base state*

The borderline between the regime for which erosion extends infinitely far upstream ($E_n > 0$) and the regime for which it does not is given by the condition $\psi_n = 1$, or equivalently by the highest value of Fr_n for which $E_n = 0$,

$$Fr_n^{4/3} = \psi. \tag{4.19}$$

The two regimes are shown in figure 6. Note that the borderline between them, which denotes the condition at which the threshold shear stress for bed erosion is just barely attained at $x = -\infty$, is independent of the exponent γ.

In figures 7 and 8 the variation of the parameters c and b as functions of Fr_n and ψ are shown for the cases $\gamma = 1.5$ and 2.0. In general larger values of Fr_n and smaller values of ψ are seen to favour larger values of the upstream wave speed c. Recall, however, that neither of these two parameters can exceed unity and yield physically realistic solutions.

Example profiles for bed elevation η and flow velocity are shown for two base-state solutions in figure 9. In the first of these, for which erosion does not extend infinitely far upstream, $\gamma = 1.5$, $\sigma = 0.1$ ($Fr_n = 0.316$) and $\psi = 0.3$. In the second, for which

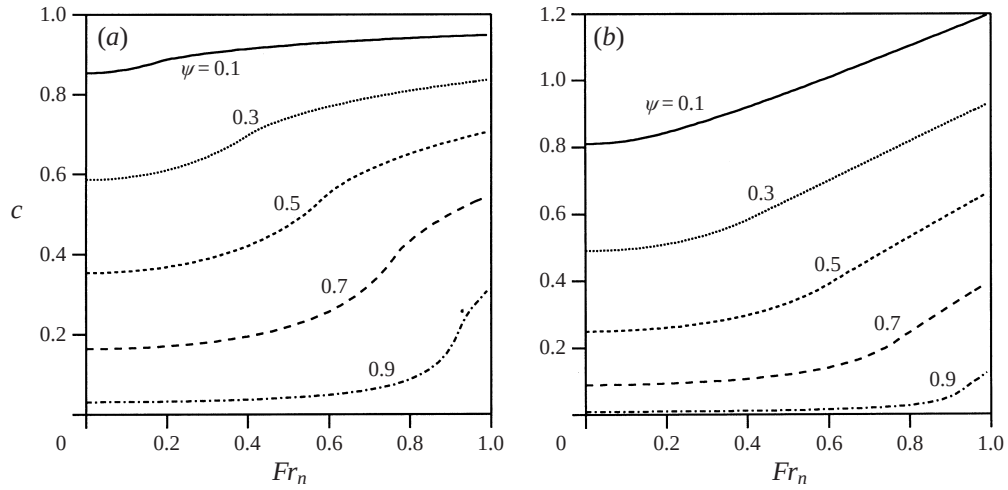

FIGURE 7. Plot of c as a function of Fr_n and ψ for (*a*) $\gamma = 1.5$ and (*b*) $\gamma = 2.0$.

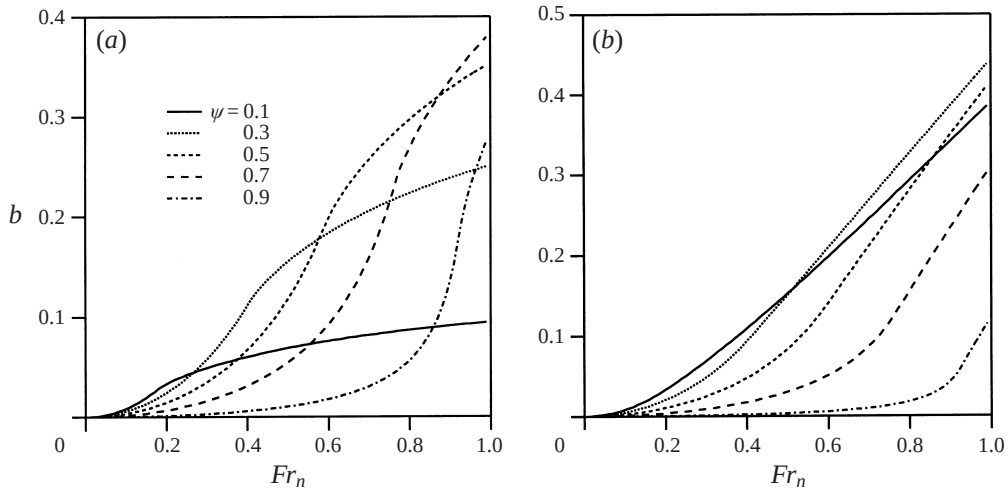

FIGURE 8. Plot of b as a function of Fr_n and ψ for (*a*) $\gamma = 1.5$ and (*b*) $\gamma = 2.0$.

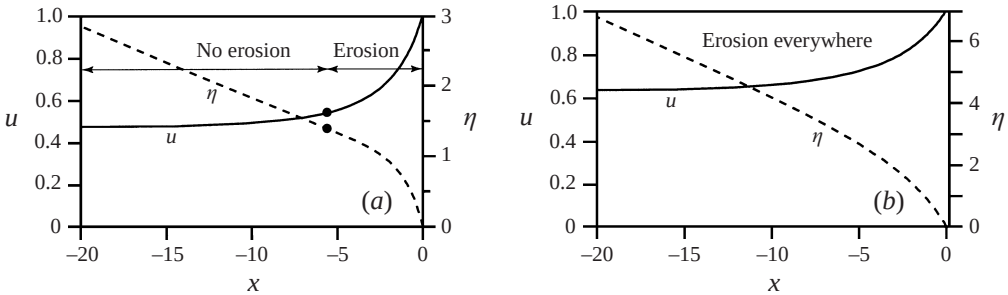

FIGURE 9. (*a*) Plot of u and η versus x for $\gamma = 1.5$, $\sigma = 0.1$ and $\psi = 0.3$. Note that erosion does not extend infinitely far upstream in this case. (*b*) As (*a*) but for $\sigma = 0.25$. Note that erosion extends infinitely far upstream in this case.

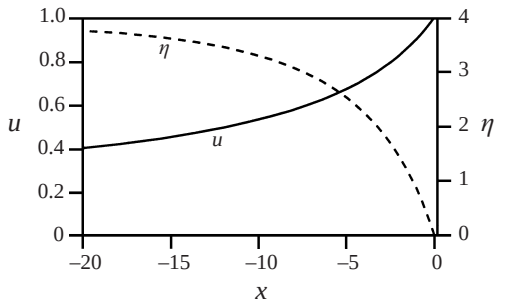

FIGURE 10. Plot of u and η versus x for $\gamma = 1.5$, $\sigma = 0$ and $\psi = 0.1$. Note that bed slope converges to zero a finite distance upstream, but u converges to zero only as $x \to \infty$.

erosion extends infinitely far upstream, $\gamma = 1.5$, $\sigma = 0.25$ ($Fr_n = 0.5$) and $\psi = 0.3$. It should be recalled that the parameters used in the non-dimensionalization for bed elevation versus distance are inherently greatly distorted, with elevation made dimensionless with the scale D_c and streamwise distance made dimensionless with the scale D_c/C_f.

It is of some interest to note that the analysis for the base state is well behaved even in the limit as $\sigma \to 0$ (in which case $Fr_n \to 0$ as well). In this case the bed slope converges to zero a finite distance upstream of $x = 0$, but flow velocity u converges to zero only as $-x \to \infty$. A sample calculation is shown for the case $\gamma = 1.5$, $\sigma = 0$ ($Fr_n = 0$) and $\psi = 0.1$ in figure 10.

5. Perturbation and linear stability analysis

5.1. *Linearization*

Having specified the base state, it is now possible to proceed to the linear stability analysis for incipient channellization. In the analysis that follows the subscript 0 is used to denote the base state, so that u_0 and η_0 denote flow velocity and bed elevation of the base state. The dimensionless formulation of the previous section is retained here.

A laterally undulating perturbation is now added to the base state in accordance with the description of figure 4. Since the perturbation is imbedded in a landscape that is moving upstream at speed c, the problem can be formulated directly in terms of the moving coordinate system. The perturbation can be conceptualized as incipient gullies originating from the Froude-critical point, where the bed elevation now takes the initial form

$$\eta = a\cos ky \quad \text{at} \quad t = 0,\ x = 0. \tag{5.1}$$

Here a is perturbation amplitude at $t = 0$, which is taken to be arbitrarily small. The question of interest here is whether or not such an initial perturbation reinforces itself, thus causing amplitude to grow and the channellization of figure 4 to commence, or the perturbation dies, restoring the base sheet flow.

Equations (3.14)–(3.16) remain unchanged in the dimensionless moving coordinate system; (3.17) now reduces with the aid of (4.4) and (4.7) to the form

$$\frac{\partial \eta}{\partial t} + c\frac{\partial \eta}{\partial y} + c\sigma + E(u^2 + v^2) - E(\sigma^{2/3}) = 0, \tag{5.2}$$

where $E(\sigma^{2/3})$ is identical with the parameter E_n. The following forms are now

introduced to describe the perturbations in u, v, h and η to $O(a)$:

$$u = u_0 + au_1 + \cdots, \qquad v = av_1 + \cdots, \tag{5.3a,b}$$

$$h = h_0 + ah_1 + \cdots, \qquad \eta = \eta_0 + a\eta_1 + \cdots. \tag{5.3c,d}$$

Note that in the above relations, the $O(1)$ parameters of the base state are functions of x only, whereas the $O(a)$ perturbations are functions of x, y and t. Substituting these relations into (3.14)–(3.16) and (5.2) and expanding, the following results are obtained.

At $O(1)$ in a the formulation of the base state is precisely recovered, as expected:

$$u_0 \frac{\mathrm{d}u_0}{\mathrm{d}x} = -\frac{\mathrm{d}h_0}{\mathrm{d}x} - \frac{\mathrm{d}\eta_0}{\mathrm{d}x} - \frac{u_0^2}{h_0}, \tag{5.4}$$

$$u_0 h_0 = 1, \tag{5.5}$$

$$c\frac{\mathrm{d}\eta_0}{\mathrm{d}x} + c\sigma + E(u_0^2) - E(\sigma^{2/3}) = 0. \tag{5.6}$$

At $O(a)$ in a the following forms are obtained:

$$u_0 \frac{\partial u_1}{\partial x} + u_0' u_1 = -\frac{\partial h_1}{\partial x} - \frac{\partial \eta_1}{\partial x} - 2u_0^2 u_1 + u_0^4 h_1, \tag{5.7}$$

$$u_0 \frac{\partial v_1}{\partial x} = -\frac{\partial h_1}{\partial y} - \frac{\partial \eta_1}{\partial y} - u_0^2 v_1, \tag{5.8}$$

$$h_0 \frac{\partial u_1}{\partial x} + h_0' u_1 + u_0 \frac{\partial h_1}{\partial x} + u_0' h_1 + h_0 \frac{\partial v_1}{\partial y} = 0, \tag{5.9}$$

$$\frac{\partial \eta_1}{\partial t} + c\frac{\partial \eta_1}{\partial x} + E_u(u_0^2) u_1 = 0. \tag{5.10}$$

In the above relations the prime denotes the ordinary derivative of a base-state variable with respect to x, and the subscript u denotes a derivative with respect to u. Thus the parameter $E_u(u_0^2)$ is given by

$$E_u(u_0^2) = \begin{cases} 2\gamma(u_0^2 - \psi)^{\gamma-1} u_0 & \text{if } u_0^2 \geqslant \psi \\ 0 & \text{if } u_0^2 < \psi. \end{cases} \tag{5.11}$$

Note that in (5.11), when $\gamma < 1$ the parameter E_u attains an infinite value wherever $u_0^2 = \psi$. This implies that the domain to the left of the dividing line in figure 6 cannot be realistically described for the case $\gamma < 1$. Here the analysis is restricted to the range $\gamma \geqslant 1$, and to values of γ within this range which yield positive values of u_{x0} from (4.18).

Separable solutions to (5.7)–(5.10) are represented as follows:

$$u_1 = u_1^*(x)\,\mathrm{e}^{\omega t}\cos ky, \qquad v_1 = v_1^*(x)\,\mathrm{e}^{\omega t}\sin ky, \tag{5.12a,b}$$

$$h_1 = h_1^*(x)\,\mathrm{e}^{\omega t}\cos ky, \qquad \eta_1 = \eta_1^*(x)\,\mathrm{e}^{\omega t}\cos ky, \tag{5.12c,d}$$

where ω denotes the time growth rate of the amplitude of the initial perturbation. Note that the base state is unstable, and incipient channellization amplifies itself when $\omega > 0$. Substituting (5.12) into (5.7)–(5.10) and reducing, the following ordinary

differential equations are obtained for the starred quantities in (5.12):

$$\frac{\mathrm{d}u_1^*}{\mathrm{d}x} = \frac{(u_0^2 + u_0^{-1})u_0' + 2u_0^4 - c^{-1}E_u(u_0^2)u_0^2}{1 - u_0^3}u_1^* - \frac{k}{1 - u_0^3}v_1^* - \frac{u_0u_0' + u_0^6}{1 - u_0^3}h_1^* - \frac{c^{-1}\omega u_0^2}{1 - u_0^3}\eta_1^*, \tag{5.13}$$

$$\frac{\mathrm{d}v_1^*}{\mathrm{d}x} = -u_0v_1^* + \frac{k}{u_0}h_1^* + \frac{k}{u_0}\eta_1^*, \tag{5.14}$$

$$\frac{\mathrm{d}h_1^*}{\mathrm{d}x} = -\frac{2u_0' + 2u_0^2 - c^{-1}E_u(u_0^2)}{1 - u_0^3}u_1^* + \frac{ku_0}{1 - u_0^3}v_1^* + \frac{u_0^4 + u_0^2u_0'}{1 - u_0^3}h_1^* + \frac{c^{-1}\omega}{1 - u_0^3}\eta_1^*, \tag{5.15}$$

$$\frac{\mathrm{d}\eta_1^*}{\mathrm{d}x} = -c^{-1}E_u(u_0^2)u_1^* - c^{-1}\omega\eta_1^*. \tag{5.16}$$

5.2. *Boundary conditions*

Here it is assumed that far upstream the perturbations die out, so that the base solution is realized as $x \to -\infty$. (In point of fact only two conditions can be realized far upstream: either the perturbations die out or they become infinitely large. The latter case is excluded here on physical grounds.) Thus the following conditions are imposed:

$$u_1^* = 0, \quad v_1^* = 0, \quad h_1^* = 0, \quad \eta_1^* = 0 \qquad \text{as} \quad x \to -\infty. \tag{5.17a–d}$$

An examination of the structure of (5.13)–(5.16) reveals, however, that if three of the above conditions are imposed, with fourth one is satisfied identically. Thus in reality only three independent boundary conditions are specified by the above relations.

The condition of Froude-critical flow at the downstream boundary of the flow domain is preserved in the present analysis. The downstream boundary, however, is no longer precisely at $x = 0$ in the light of the perturbations. Non-dimensionalizing (3.8*a*), the following condition holds:

$$\frac{u^2 + v^2}{h} = 1 \quad \text{at} \quad x = a\chi\cos ky, \tag{5.18}$$

where the quantity $a\chi\cos ky$ denotes the perturbed position of the Froude-critical point consonant with the forms (5.12). Substituting (5.3) and (5.12) into (5.18) and reducing, at $O(1)$ in a it is found that

$$u_0 = h_0 \quad \text{at} \quad x = 0. \tag{5.19}$$

Since by definition $u_0(0) = h_0(0) = 1$, the boundary condition is satisfied identically as part of the base flow solution. The following relation is obtained at $O(a)$ in a:

$$2u_1^* + 2u_0'\chi = h_1^* + h_0'\chi \quad \text{at} \quad x = 0. \tag{5.20}$$

Noting from (5.5) that $u_0'(0) + h_0'(0) = 0$, the above relation is quickly reduced to

$$2u_1^* + 3u_0'\chi = h_1^* \quad \text{at} \quad x = 0. \tag{5.21}$$

The downstream boundary condition thus becomes the relation by which the unknown

χ, and thus the effect of the perturbations on the position of the Froude-critical point, is evaluated.

In the light of the specification (5.1), the parameter η_1^* must be normalized so as to satisfy the following condition at the origin:

$$\eta_1^* = 1 \quad \text{at} \quad x = 0. \tag{5.22}$$

In this way three of the relations (5.17) and (5.22) specify four boundary conditions on the four unknowns u_1^*, v_1^*, h_1^* and η_1^* of (5.13)–(5.16). In point of fact, however, these equations contain a fifth unknown, namely the perturbation growth rate ω. Thus one more condition is needed to close the problem. Once this condition has been specified, the problem can be solved, and the effect of the perturbations on the Froude-critical point can be evaluated from (5.21).

5.3. *Regularity condition*

It was noted in the discussion of the base flow solution that at $x = 0$ the denominator $1 - u^3$ ($1 - u_0^3$ in the notation of this section) of (4.17) vanishes. The condition for the existence of a non-singular solution is that the numerator must vanish as well. The same problem arises at $O(a)$, as can be seen from an examination of (5.13) and (5.15). For example, (5.13) may be rewritten as

$$(1 - u_0^3)\frac{\mathrm{d}u_1^*}{\mathrm{d}x} = [(u_0^2 + u_0^{-1})u_0' + 2u_0^4 - c^{-1}E_u(u_0^2)u_0^2]u_1^* - kv_1^* - (u_0u_0' + u_0^6)h_1^* - c^{-1}\omega u_0^2\eta_1^*. \tag{5.23}$$

Note that if $\mathrm{d}u_1^*/\mathrm{d}x$ is to be non-singular at the origin, it follows that the right-hand side of (5.23) must vanish there, yielding with the aid of (5.22) the regularity condition

$$[E_u(1) - 2c(p+1)]u_1^* + kcv_1^* + c(p+1)h_1^* + \omega = 0 \quad \text{at} \quad x = 0, \tag{5.24}$$

where $p = u_0'(0) = u_{x0}$. The same analysis as applied to (5.15) yields exactly the same relation, so that (5.24) provided the fifth condition needed to evaluate the five parameters u_1^*, v_1^*, h_1^*, η_1^* and ω.

5.4. *Method of solution*

Equations (5.13)–(5.16) have solutions satisfying the boundary and regularity conditions only for particular values of ω, and thus the equations and conditions define an eigenvalue problem. With this in mind it is possible to reduce the problem to an equivalent two-point boundary value problem associated with the points $x = 0$ and $x = -\infty$. Insofar as the equations do not obviously admit an analytical solution, a numerical method is used here. In particular, the equations are solved using the relaxation method outlined in Press *et al.* (1992).

6. Results and observations

6.1. *Characteristic wavenumber for maximum instability*

The instability phenomenon described here is completely characterized by the same parameters that specify the base flow, i.e. the exponent γ in the erosion relation, the normalized upstream slope σ (or the normal Froude number of the upstream flow Fr_n) and the ratio ψ of the critical shear stress for bed erosion to the shear stress at the Froude-critical condition, and one additional parameter, i.e. the transverse

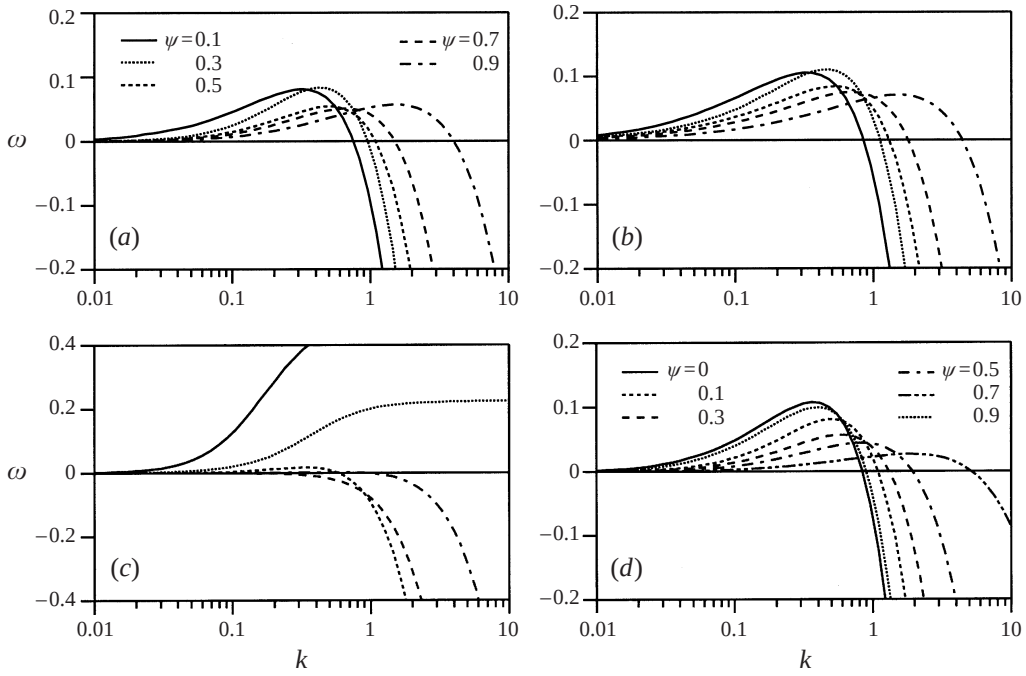

FIGURE 11. Dependence of ω on ψ and k. (*a*) $\sigma = 0.1$, $\gamma = 1.5$; (*b*) $\sigma = 0$, $\gamma = 1.5$; (*c*) $\sigma = 0.5$, $\gamma = 1.5$; (*d*) $\sigma = 0.1$, $\gamma = 2.0$.

wavenumber k of the perturbations. Thus the growth rate ω takes the following functional form:

$$\omega = \omega(\sigma, \psi, \gamma, k). \tag{6.1}$$

The dependence of ω on these parameters is studied in figures 11 and 12. The general dependence of ω on k (except within a region near $\gamma = 1.5$ and $\psi = 0$, as detailed below) can be described as follows. As k becomes small ω approaches zero. As k increases ω typically increases above zero, reaches a maximum, and then quickly drops off into the negative range for further increases in k. The values of k for positive ω are typically less than 10. Thus the following two results are obtained: (*a*) a range of wavenumbers for which ω is positive, and thus incipient channellization reinforces itself, is found for a wide range of conditions; and (*b*) the plot of ω versus k commonly possesses a value k_m associated with maximum ω, implying the selection of a preferential wavelength at the linear level. To the authors' knowledge, the present analysis is the first formal stability analysis to successfully predict wavelength selection at the linear level.

In figures 11(*a*)–11(*c*) the variation of ω in k, σ and ψ is studied for the case $\gamma = 1.5$. In the cases of figures 11(*a*) ($\sigma = 0.1$) and 11(*b*) ($\sigma = 0$) the plot of ω versus k has a wavenumber k_m somewhere between 0.3 and 0.9 associated with a positive maximum growth rate ω_m for values of ψ ranging from 0.1 to 0.7. This wavenumber constitutes the characteristic wavenumber of channellization predicted by this linear theory. Within the specified range of ψ, k_m tends to increase somewhat with increasing ψ.

In the cases described by the above three plots, a characteristic wavenumber ceases to exist in the limits $\psi \to 0$ and $\psi \to 1$. In the latter case this is because ω becomes

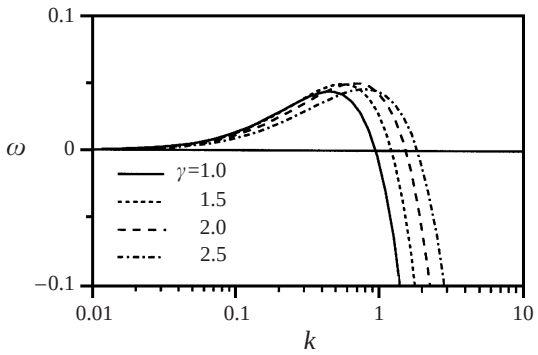

FIGURE 12. Dependence of ω on k for various values of γ, for the case $\sigma = 0.1$ and $\psi = 0.6$.

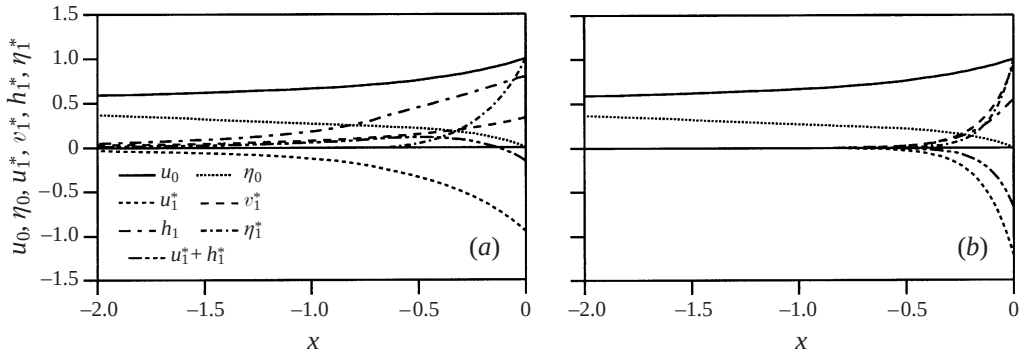

FIGURE 13. Plots of u_0, η_0, u_1^*, v_1^*, h_1^* and η_1^* are shown for $\gamma = 1.5$, $\sigma = 0.1$ and $\psi = 0.5$. (*a*) $k = 0.5$, corresponding to a maximum growth rate $\omega = 0.426$; (*b*) $k = 5.0$, yielding a value of ω of -1.25.

negative for all values of k, a result that is perhaps not unexpected in that values of ψ only slightly less than one restrict any erosion to the immediate vicinity of the Froude-critical point of the base state. In the latter case, the analysis fails as $\psi \to 0$ in the case $\gamma = 1.5$.

This failure is associated with the nature of the base solution in the specific case $\gamma = 1.5$. It can be seen from (4.18) with the aid of (3.19*c*) and (4.6) that the parameter $u_{x0} \to 0$ as $\psi \to 0$ for $\gamma = 1.5$, yielding a condition for which no base solution exists. Such a condition does not prevail for values of γ in excess of 1.5, for which the base state is well behaved as $\psi \to 0$. This is illustrated in figure 11(*d*) for the values $\gamma = 2.0$ and $\sigma = 0.1$. It is seen therein that the highest growth rate is attained for the case $\psi = 0$.

It is seen in figure 11(*c*), for which $\sigma = 0.5$ ($Fr_n = 0.707$), that no characteristic wavenumber k_m exists for sufficiently small values of ψ. In the range for which the curve of ω versus k possesses a maximum, the instability appears to be suppressed. This suppression is associated with values of σ (Fr_n) approaching unity.

In figure 12 the role of varied exponent γ in the erosion relation on the curve $\omega(k)$ is studied for the case $\sigma = 0.1$ and $\psi = 0.6$. It is seen that the variation of the curve in γ over the range from 1.0 to 2.5 is relatively modest. The characteristic wavenumber k_c increases somewhat with γ, but remains in the range 0.3–0.9.

In figures 13(*a*) and 13(*b*) the spatial variation of u_0, η_0, u_1^*, v_1^*, h_1^* and η_1^* is shown for the values $\gamma = 1.5$, $\sigma = 0.1$ and $\psi = 0.6$. In figure 13(*a*) k has been set equal to the

value of 0.5 that yields the maximum growth rate ω of 0.426 for this case. In figure 13(*b*) k has been increased to 5.0, yielding a value of ω of -1.25, i.e. well into the range for which the base state is stable. The streamwise discharge per unit width uh can be expanded with the aid of (5.3), (5.5) and (5.12) to yield the result

$$uh = 1 + a\mathrm{e}^{\omega t}\cos ky(u_0 h_1^* + u_0^{-1}u_1^*). \tag{6.2}$$

The value of this parameter at the origin is given by

$$uh|_{x=0} = 1 + a\mathrm{e}^{\omega t}\cos ky(h_1^* + u_1^*). \tag{6.3}$$

It can be seen from the two plots that u_1^*, v_1^* and $(u_1^* + h_1^*)$ are larger near the origin in the case of figure 13(*b*). That is, near the origin larger value of k favours more gathering of the flow in the troughs of the perturbations. Farther upstream, however, it is seen that the smaller value of k is more effective in gathering flow into the troughs. A competition between these two effects, one favouring larger wavenumbers and the other favouring smaller wavenumbers results in the selection of a wavenumber k_c for maximum gathering of flow in the troughs, corresponding to maximum instability, in the range 0.4–0.8.

6.2. *Spacing between incipient channels*

In most cases for which ψ or σ is not close to unity the instability leading to channellization is manifested only in the range for which k is between about 0.06 and 1, and the characteristic wavelength k_m is typically between 0.04 and 0.08. The dimensional characteristic wavelength defining the spacing between incipient channels $\tilde{\lambda}_m$ is related to k_m according to

$$\tilde{\lambda}_m = 2\pi D_c C_f^{-1} k_m^{-1}. \tag{6.4}$$

An appropriate estimate for the resistance coefficient C_f associated with sheet flow is 0.01. With this in mind the spacing $\tilde{\lambda}$ between channels must be within a range near 600 to 10 000 times the critical depth D_c in order for the channelizing instability to be manifested. Estimating the characteristic wavenumber k_m to be near 0.6, it can be concluded that the spacing between channels predicted by the present linear theory should be on the order of 1000 times D_c.

Montgomery & Dietrich (1989), Dietrich & Dunne (1993) and Izumi & Parker (1995*a*) have noted that the minimum spacing between channels on hillslopes is typically on the order of 60 to 130 m, so that an overall scaling for minimum channel spacing is $\sim$ 100 m. The first two papers discuss field sites to which the present analysis can be applied. The present analysis requires a critical depth of flow D_c of $\sim$ 0.1 m in order to realize the expected spacing ($\sim$ 100 m). In the absence of infiltration, a rainfall of 360 mm h^{-1} over a length of 1 km of hillslope can produce a discharge per unit width q at the downstream end of 0.1 m^2 s^{-1}, and thus from (3.13*c*) a value of D_c of 0.1 m s^{-1}. While such a rainfall is fairly extreme, it is likely that relatively extreme events play a controlling role in the process of channellization.

It should be noted, however, that the present theory need not precisely predict the spacing observed in the field. It is likely that nonlinear effects winnow out the weaker channels, leading to a gradual increase in channel spacing in time as compared to the one predicted for incipient channellization. A repeat of the above analysis with a rainfall rate of 70 mm h^{-1} results in an incipient spacing of about 34 m, a value that could easily increase to the order of 100 m under the influence of nonlinear effects.

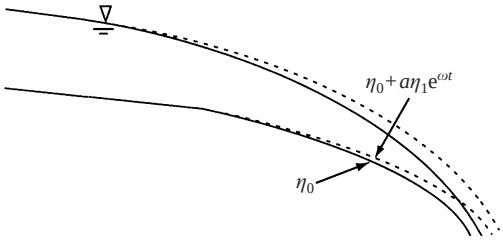

FIGURE 14. Diagram illustrating the introduction of streamwise perturbations to the base state.

6.3. *On the stability of the base state to streamwise perturbations*

The base state assumed here, i.e. a one-dimensional downward-concave hillslope profile that migrates upstream at constant rate would appear to be a reasonable starting point for the study of the inception of channellization. The base state clearly constitutes a fully nonlinear equilibrium state. If, however, this equilibrium state is unstable to streamwise perturbations, it might dissipate or devolve into a different shape before the transverse instability associated with incipient channellization has a chance to take hold. It is thus of value to consider whether the base state itself is stable to streamwise perturbations. This is especially the case in the light of the fact that Parker & Izumi (2000) have shown that under certain circumstances long profiles subject to erosion can devolve into a series of periodic steps.

With this in mind attention is briefly focused on the one-dimensional analysis associated with the base state. As shown in figure 14, this base state may be subjected to an infinitesimal perturbation at the origin such that the following condition is satisfied:

$$\eta = a \quad \text{at} \quad t = 0,\ x = 0. \tag{6.5}$$

Corresponding to (6.5) are the forms

$$u = u_0(x) + a u_1(x) e^{\omega t}, \qquad h = h_0(x) + a h_1(x) e^{\omega t}, \tag{6.6a, b}$$

$$\eta = \eta_0(x) + a\eta_1(x) e^{\omega t}, \tag{6.6c}$$

where ω denotes the growth rate of these streamwise perturbations. Substitution of (6.6) into (4.1)–(4.3) and reduction would lead to a formal stability analysis. A consideration, however, of the problem of channellization that has already been solved leads to the conclusion that the one-dimensional stability analysis already described can be obtained forthwith in the limit as $k \to 0$. As described earlier, that analysis predicts values of ω that always vanish for $\gamma \geqslant 1.5$ in this limit. The stability of the base state to streamwise perturbations helps justify its use as the starting point for an analysis of the stability of transverse perturbations associated with incipient channellization.

7. Discussion

Two issues merit further discussion. The first of these refers to the range of validity of the present downstream-driven theory of channellization. Since the theory applies to a base state that attains subcritical flow far upstream, the theory cannot be used to explain channellization occurring on slopes steep enough to support supercriticality everywhere. This does not imply that channellization does not occur under such conditions, but rather that it is driven by a different mechanism. For

example, upstream-driven theory of channellization due to Izumi & Parker (1995*a*) is applicable to such conditions. Although the mechanism of channellization is different, the spacing between channels predicted by that theory is of the same order of magnitude as that predicted by the present theory. In addition, there is a certain consistency in an overall picture according to which channellization is driven from the upstream end under Froude-supercritical conditions and from the downstream end (or upstream end) under Froude-subcritical conditions.

The second issue concerns the downstream-driven theory of channellization of Izumi & Parker (1995*b*), which is superseded by the present analysis. In that formulation flow over the free overfall illustrated in figure 2 was considered. It was found in the analysis that if conditions precisely at the precipice were considered, the incipient spacing between channels declines to zero. In order to obtain a finite spacing, it was necessary to consider the incipient pattern of erosion somewhat upstream of the precipice, where the boundary shear stress first becomes equal to the threshold value for bed erosion. While the analysis considers the same mechanism the present one, the assumption of a vertical precipice made it impossible to cast the treatment in the form of a rigorous stability analysis, and in addition required the introduction of an element of subjectivity. Vertical precipices in cohesive soil may be briefly created by tectonic processes, but weathering and soil erosion should quickly smear these out. The self-preserving downward-concave profile used here defines a far more realistic base state, and makes possible a formal stability analysis. The key to the successful analysis is the regularity condition (4.18), which ensures a finite, positive value of the streamwise rate of change of flow velocity u_{x0} at the Froude-critical point. In the case of a free overfall the Froude-critical point is reached as the precipice, where u_{x0} becomes infinitely large.

8. Conclusions

A formal stability analysis for downstream-driven incipient channellization on hillslopes is presented. The analysis relies on a base state that consists of a Froude-subcritical sheet flow over an eroding, downward-concave bed profile migrating slowly upstream at constant speed. Channellization is driven from the point at the downstream end of the domain where the flow of the base state obtains the critical Froude number of unity. The analysis predicts the following.

The base profile is stable to streamwise perturbations. Solutions can be found both for the case when erosion extends infinitely far upstream of the Froude-critical point, and when it extends only a finite distance upstream. Far upstream the flow reaches an equilibrium state with a normal Froude number Fr_n that must be less than unity. Solutions can also be found for the limit $Fr_n \rightarrow 0$, in which case the bed slope far upstream becomes vanishing.

A range of conditions exist for which the base state is unstable to perturbations in the transverse direction consisting of a series of troughs and ridges aligned downstream. The instability is manifested if the following two parameters are sufficiently smaller than unity: (*a*) the upstream normal Froude number Fr_n and (*b*) the ratio ψ of critical stress for bed erosion to the boundary shear stress of the base state attained at the Froude-critical point. Singular behaviour as e.g. $Fr_n \rightarrow 0$ can be avoided as long as the exponent γ in the erosion relation exceeds 1.5.

The instability describes incipient channellization. It appears for values of dimensionless wavenumber k between roughly 0.06 and 1, and is maximized for a value k_m that is typically close to 0.6. Assuming a friction factor C_f of the order of 0.01

and appropriate rates of runoff corresponding to intense storms, this translates to a spacing between incipient channels of 30 to 100 m.

It can be expected that nonlinear processes should winnow out the weaker channels, and result in a spacing that is larger than that prevailing under incipient conditions.

The present analysis cannot explain channellization on slopes so steep that Froude-supercritical flow is maintained over a substantial distance. The upstream-driven analysis of Izumi & Parker (1995*a*), however, applies to this case. It predicts a spacing between channels that is of the same order of magnitude as that predicted here.

The contribution of the second author to this work was supported by the US National Science Foundation (grant no. CTS-9424507).

REFERENCES

Ariathurai, R. & Arulanandan, K. 1978 Erosion rates of cohesive soils. *Proc. ASCE, Journal of Hydraulic Division* **104(HY2)**, 279–283.

Chow, V. T. 1959 *Open-Channel Hydraulics.* McGraw-Hill.

Dietrich, W. E. & Dunne, T. 1993 The channel head. In *Channel Networks Hydrology* (ed. K Berlin & M. J. Kirkby), pp. 175–219. Wiley.

Escoffier, F. F. 1958 Transition profiles in nonuniform chanels. *Trans. ASCE* **123**, 43–56.

Howard, A. D. 1994 A detachment-limited model of drainage basin evolution. *Wat. Resour. Res.* **30**, 2261–2285.

Izumi, N. & Parker, G. 1995*a* Inception of channellization and drainage basin formation: upstream-driven theory. *J. Fluid Mech.* **283**, 341–363.

Izumi, N. & Parker, G. 1995*b* On incipient channels formed at the downstream end of plateaux. *J. Hydraul. Coastal Environ. Engng, JSCE* **521**, 79–91, in Japanese.

Loewenherz, D. S. 1991 Stability and the initiation of channellized surface drainage: a reassessment of the short wavelength limit. *J. Geophys. Res.* **96**, 8453–8464.

Luke, J. 1974 Special solutions for nonlinear erosion problems. *J. Geophys. Res.* **79**, 4035–4040.

Montgomery, D. R. & Dietrich, W. E. 1989 Source area, drainage density and channel initiation. *Wat. Resour. Res.* **25**, 1907–1918.

Parker, G. & Izumi, N. 2000 Purely erosional cyclic and solitary steps created by flow over a cohesive bed. *J. Fluid Mech.*, **419** 203–238.

Press, H. P., Teukolsky, S. A., Vetterling, W. T. & Flannery, B. P. 1992 *Numerical Recipes in FORTRAN*, 2nd Edn. Cambridge University Press.

Reid, L. M. 1989 Channel incision by surface runoff in grassland catchments. PhD thesis, University of Washington.

Rodriguez-Iturbe, I. & Rinaldo, A. 1997 *Fractal River Basins: Chance and self-Organization.* Cambridge University Press.

Sawai, K. 1977 Sediment hydraulics research on the mechanism of variation of the bed of cohesive channels. PhD thesis, Kyoto University.

Sheng, Y. P. & Lick, W. 1978 The transport and resuspension of sediments in a shallow lake. *J. Geophys. Res.* **84**, 1809–1826.

Smith, T. & Bretherton, F. B. 1972 Stability and the conservation of mass in drainage basin evolution. *Wat. Resour. Res.* **8**, 1506–1529.

Tucker, G. & Slingerland, R. 1997 Drainage basin responses to climate changes. *Wat. Resour. Res.* **33**, 2031–2047.

Willgoose, G., Bras, R. L. & Rodriguez-Iturbe, I. 1991*a* A coupled channel network growth and hillslope evolution model. 1. Theory. *Wat. Resour. Res.* **27**, 1671–1684.

Willgoose, G., Bras, R. L. & Rodriguez-Iturbe, I. 1991*b* A coupled channel network growth and hillslope evolution model. 2. Nondimensionalization and applications. *Wat. Resour. Res.* **27**, 1685–1696.